Noname manuscript No.
(will be inserted by the editor)

Machine Learning Deriven Set of microRNAs as a Novel Biomarker for Myocardial Infarction Diagnosis

Mehrdad Samadishadlou · Reza Rahbarghazi · Farhad Bani ·

Received: date / Accepted: date

Abstract MicroRNAs (miRNAs) play a crucial role in regulating adaptive and maladaptive responses in cardiovascular diseases, making them attractive targets for potential therapeutics. However, their potential as novel biomarkers for diagnosing cardiovascular diseases needs to be evaluated systematically. In this study, we aimed to identify a key set of miRNA biomarkers using integrated bioinformatics and machine learning analysis. We combined and analyzed three gene expression datasets from the Gene Expression Omnibus (GEO) database, which contained peripheral blood mononuclear cells samples from individuals with myocardial infarction (MI), stable coronary artery disease (CAD), and healthy. Additionally, we selected a set of miRNAs based on their area under the curve of the receiver operating characteristic (AUC-ROC) for separating CAD/MI samples. We designed a two-layer architecture for sample classification, with the first layer isolating healthy samples from not-healthy ones, and the second layer classifying stable CAD and MI samples. We trained different machine learning models using both biomarker sets and evaluated their performance on a test set. We identified miR-21, miR-186, and miR-32 as the only miRNAs in the differentially expressed genes, and a set included miR-21, miR-155, miR-142, miR-197, miR-29A, and miR-320C1 as the optimum set of miRNA selected by their AUC-ROC. Both biomarker sets were able to distinguish healthy from not-healthy samples with complete

Mehrdad Samadishadlou
Medical Nanotechnology gruop, Tabriz University of Medical Sciences, Tabriz, Iran
E-mail: samadishadlou@tbzmed.ac.ir

Reza Rahbarghazi
Medical Nanotechnology gruop, Tabriz University of Medical Sciences, Tabriz, Iran
E-mail: rahbarghazir@tbzmed.ac.ir

Farhad Bani
Medical Nanotechnology gruop, Tabriz University of Medical Sciences, Tabriz, Iran
E-mail: bainf@tbzmed.ac.ir

accuracy. The best performance for classification of CAD and MI was achieved with an SVM model trained using the biomarker set selected by AUC-ROC, with an AUC of 0.95 and an accuracy of 0.88. Our study demonstrates that miRNA signatures derived from peripheral blood could serve as valuable novel biomarkers for cardiovascular diseases.

Keywords microRNA · Machine Learning · Myocardial Infarction ·

1 Introduction

At present, cardiovascular diseases (CVDs) are the leading cause of human mortality with 32% of all global deaths. It is estimated that about 85% of CVDs mortality were diagnosed with myocardial infarction (MI) ("Cardiovascular Diseases (CVDs)" n.d.). MI is an acute coronary syndrome with sudden blockage and stenosis of the coronary artery, and subsequent myocardial ischemia, leading to extensive cardiomyocyte damage and necrosis (Yap et al. 2023).

Over the last 50 years, numerous attempts have been collected to use biomarkers to facilitate diagnosis, assess risk, follow-up therapy, and determine therapeutic efficacy in CVDs candidates. Based on the released guidelines, cardiac troponins (cTns) are used as a highly-sensitive and accurate approach for the detection of myocardial ischemia. Despite the inherent advantages, the high-rate sensitivity of cTn-based assays has also led to more false positive results (Thygesen et al. 2018), which do necessitate the advent and development of new modalities with pathological values. To improve diagnostic value upon existing CVD biomarkers, the combination of complementary biological markers, such as microRNAs (miRNAs) and other genetic factors, is proposed. Previous data support the notion that miRNAs exhibit the great potential to be used as alternative biomarkers in CVD detection and follow-up (Schulte et al. 2020). It is suggested that miRNAs possess 18-22 nucleotides and can play a crucial role in the regulation of gene expression. Evidence point to the fact that miRNAs are involved in the pathogenesis of cardiac tissue injury and be as theranostics in terms of CVDs. These elements can easily circulate in biofluids with both diagnostic as well as prognostic values (Schulte, Karakas, and Zeller 2017). Several biological activities such as angiogenesis, cardiomyocyte growth and contractility, lipid metabolism, plaque formation, and cardiac rhythm are regulated by miRNAs (Kalayinia et al. 2021). It is postulated that the function and diagnostic properties of miRNAs are beyond the myocardium in CVD patients. To be specific, the expression of miRNAs can vary in different biofluids and cell components such as serum and peripheral blood mononuclear cells (PBMCs) (Soler-Botija, Gálvez-Montón, and Bayés-Genís 2019).

PBMCs are a fraction of white blood cells (WBCs), including monocytes, lymphocytes, macrophages, and other cells belonging to the immune system (Gao et al. 2020). Emerging data have indicated that PBMCs can be used as a valid source of biomarkers for monitoring various pathological conditions.

Of note, the alteration of mRNAs and miRNAs under pathological conditions gives us valuable information about different kinds of disorders. PBMCs could recapitulate the conditions of the target tissues, thus, providing a highly sensitive and specific source of biomarkers (Mosallaei et al. 2022). Commensurate with these conditions, these cells are repositories of dysregulated genes and miRNAs expression profiles in CVDs related to control conditions (Gao et al. 2020; Mosallaei et al. 2022).

In recent years, the advent and use of machine learning (ML) is an exciting prospect for advancing scientific discoveries. Although the concept of ML and its initial algorithms were conceived many years ago, recent improvements in computing power and access to vast amounts of data have shown that ML techniques outperform classical statistical methods in various fields. Furthermore, the progress made in omics technologies has enabled the analysis of massive and intricate biological data sets, consisting of hundreds to thousands of samples, which makes it possible for ML to extract valuable biological information from such data (Torun et al. 2023). Therefore, ML offers novel techniques to integrate and analyze the various omics data enabling the discovery of de novo biomarkers. These biomarkers help us in accurate disease prediction, patient stratification, and finding new therapeutics (Reel et al. 2021).

In this study, we aimed to identify potential miRNA biomarkers for MI patients by combining and analyzing three different microarray datasets from PBMCs. It is suggested that the integration of omics data with bioinformatics and ML techniques could be a promising tool in the discovery of new and more accurate biomarkers for monitoring CVDs. Besides, this approach can deepen our vision into the underlying mechanisms of CVDs and aid in the development of valid theranostic tools, and patient stratification.

2 Materials and Methods

2.1 Microarray data collection

Microarray datasets were obtained from the Gene Expression Omnibus (GEO) database (`https://www.ncbi.nlm.nih.gov/geo/`). To obtain sufficient classification power between MI, healthy and CAD samples, a relatively large sample size was required. Therefore, GSE59867 for MI and CAD samples, and GSE56609 and GSE54475 for healthy samples were selected. All samples were produced using Affymetrix Human Gene 1.0 ST Array (GPL6244) platform. Only healthy, stable CAD and early-stage MI samples were selected from these datasets for further analyses. The basic information for the three datasets evaluated in the current study is provided in Table @ref(tab:datasets).

Table 1: Basic information of the GEO microarray datasets.

Dataset	Platform	Healthy	CAD	MI	Refrence
GSE59867	GPL6244	-	46	111	(Maciejak et al. 2015)
GSE56609	GPL6244	46	-	-	(Matone et al. 2015)
GSE54475	GPL6244	5	-	-	(Canali et al. 2014)

2.2 Pre-processing

Raw data (CEL files) of all datasets were downloaded from the GEO and pre-processed using the fRMA package (M. N. McCall, Bolstad, and Irizarry 2010). fRMA allowed to pre-process of individual microarray samples and combining them consistently for analysis. For each dataset, background correction was performed using the RMA algorithm and then it was quantile normalized based on the reference distribution. During summarization, batch effects were removed and variances of the gene expressions were estimated by taking into account these probe-specific effects. For those multiple probe sets matched to the identical gene, the mean log fold change was retained. Therefore, fRMA can be seen as a batch effect removal technique for different datasets that are produced by identical microarray platforms. Thus, to ensure batch effect removal, the principal component analysis and the relative log expression of train samples were plotted before and after fRMA (Lazar et al. 2013).

2.3 Differential expression analysis

The barcode algorithm proposed by McCall et al. (Matthew N. McCall et al. 2011) transformed the actual expression values into binary barcode values. Huge sets of samples were collected and normalized using fRMA for several platforms as well as for Affymetrix Human Gene 1.0 ST Array (GPL6244) platform. The distribution of the expressed and unexpressed observed intensities for each gene is estimated using these normalized sets. Genes were considered expressed (and their value coded to 1) or unexpressed (and their value coded to 0) according to the following equation:

$$\hat{x}_{ij} = \begin{cases} 1 \text{ if } x_{ij} >= \mu^{ne} + C \times \sigma^{ne} \\ 0 \text{ otherwise} \end{cases}$$

where x_{ij} is the normalized intensity of gene i in sample j, C is a user-defined parameter, σ^{ne} is the standard deviation of the non-expressed distribution, and μ^{ne} is the mean of the non-expressed distribution. The barcode representation of a sample is a vector of ones and zeros denoting which genes are estimated to be expressed (ones) and unexpressed (zeros). The barcode algorithm was implemented by the barcode function in the R fRMA package, and the default value of C was used.

To determine if the expressed ratios differed in the MI group versus the healthy control group, Fisher's exact test for individual genes was carried out upon the barcode values. Genes with a false discovery rate (FDR) of < 0.05, which was calculated through the Benjamini-Hochberg (BH) procedure to adjust for multiple testing issues, were considered as differentially expressed genes. The same procedures were conducted on CAD versus healthy controls as well as MI versus CAD group to find the DEGs between them.

2.4 Functional and pathway enrichment analyses

Using the R clusterProfiler package, the Kyoto Encyclopedia of Genes and Genomes (KEGG) pathway enrichment analysis and Gene Ontology (GO) functional annotation were carried out on the differentially expressed genes. The GO analysis included biological process (BP), cellular component (CC) and molecular function (MF) categories. An adjusted p-value of less than 0.05 was considered to indicate a statistically significant difference. Enrichments were conducted on the MI-healthy and CAD-healthy DEGs. In these analyses, all default parameters were used.

2.5 ML procedure

The ML analysis was performed using Python software, ver. 3.9, Numpy (Harris et al. 2020), pandas (McKinney 2010), and Scikit-Learn packages (Pedregosa et al. 2011). Whenever hyper-tuning was needed, the scikit-opt package (Head et al. 2021) was used. In all ML analyses, the datasets were divided into train and test sets by a 0.7:0.3 ratio and all reported results are the average of 10-fold cross-validation.

Two different approaches were used for selecting miRNAs for model training. The first approach was using the miRNAs that are differentially expressed. In the second approach, miRNAs were selected by their individual AUC-ROC. Having the result of these two different approaches can provide an informative comparison between the predictive capabilities of sets of miRNAs selected with different logics.

2.5.1 miRNAs in DEGs

In this approach, a two-layer architecture was deployed to the data to maximize the prediction values. The first layer predicted whether a sample is healthy or not, and the second layer separated MI from CAD in the samples which were predicted as not healthy in the first layer. To this end, a distinct ML model was trained for each layer. Since there is a limited number of miRNAs in DEGs, both layers were trained with all of them. For further comparison with the models' performance, the ROC curve of each miRNA for classifying healthy and not-healthy, as well as CAD and MI, were generated using a Logistic Regression model.

First layer for isolation of healthy and not-healthy samples: An SVM model using RBF kernels was trained and hyper-tuned using all miRNAs in DEGs. To handle the severe imbalance in the number of samples (51 for the healthy and 157 for the not-healthy groups), the sample weight for the healthy and the not-healthy samples were set to 1 and 0.5, respectively.

Second layer for seperating MI and CAD samples: For the sake of reaching the highest classification performance using the set of miRNAs, different models were investigated. To do so, SVM (with linear, polynomial, and RBF kernels), Logistic Regression (LR), Random Forests (RF), k-Nearest Neighbor (kNN), Gradient Boosting (GB), XGBoost (XGB) and Decision Tree (DT) models were trained. All models were trained with their pre-set parameters with 10-fold cross-validation. The criteria for choosing the best model were the highest accuracy and AUC on the test set. The best model was hyper-tuned with the scikit-opt package (Head et al. 2021) to get the best predictive performance.

2.5.2 miRNAs with the highest AUC-ROC

Like the previous approach, a two-layers strategy was conducted. The first layer classified samples into healthy and not-healthy, and the separated MI and CAD samples. However, to keep the number of miRNAs as low as possible miRNAs were selected from the second layer (which are the miRNAs with the best performance in MI/CAD separation), and then their performance wase evaluated in the first layer. AUC-ROC of all miRNAs for classifying MI and CAD samples were calculated. To find the number of miRNAs with the highest predictive values, the miRNAs with the highest individual AUC-ROC were added to the set one by one, and the AUC-ROC for the set was calculated. The set with the highest AUC-ROC was selected for the following steps. The ROC curves for each selected miRNA for separating healthy samples from not-healthy and MIs from CADs were also plotted for further comparison.

First layer for the detection of healthy and not-healthy samples: An SVM model with an RBF kernel was trained using the selected set of miRNAs. Additionally, the model was hyper-tuned to find the hyper-parameters for the highest AUC and accuracy. The ROC curve and confusion matrix for the best model were reported.

Second layer for separating MI and CAD: The selected miRNAs set was used to train different algorithms to find the best model. Similar to the previous approach, SVM (with linear, polynomial, and RBF kernels), LR, RF, kNN, GB, XGB, and DT were trained. All models were trained with their pre-set parameters using 10-fold cross-validation. The models with the highest AUC-ROC and accuracy on the test set were selected and hyper-tuned using the scikit-opt package (Head et al. 2021). The ROC curve and confusion matrix for the best model were reported.

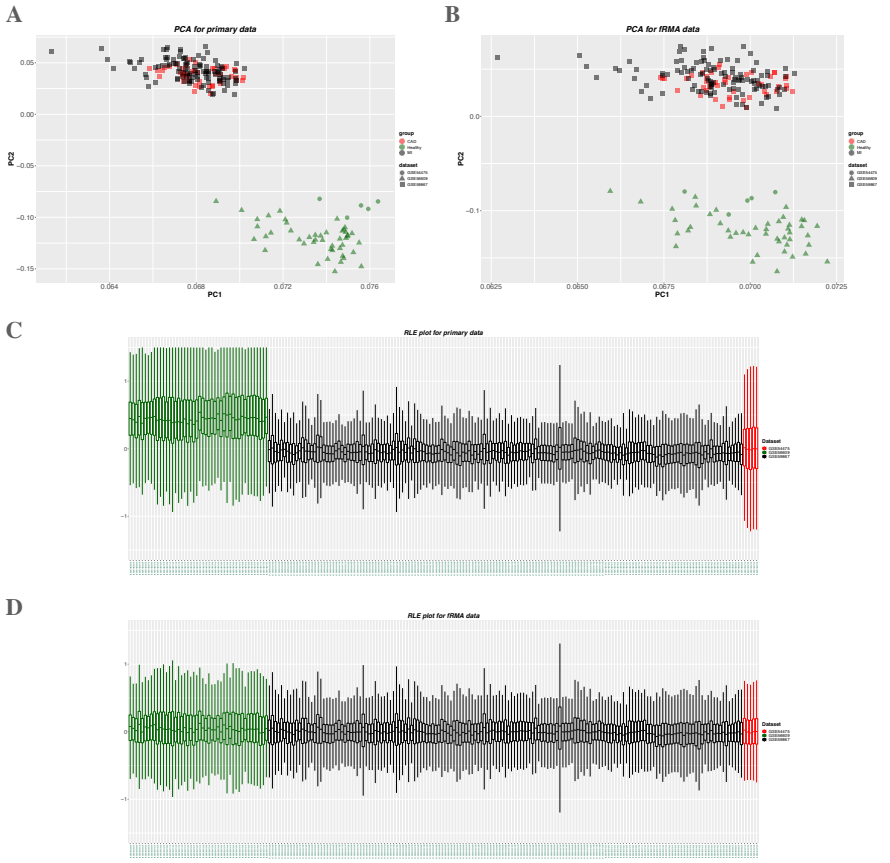

Fig. 1 PCA and RLE plot for all samples before and after fRMA.

3 Results

3.1 Pre-processing

The PCA plots of the training samples are shown in Figure @ref(fig:PCA)A and B. As shown, healthy samples were separated from CAD or MI samples in primary data and also after conducting fRMA. In the RLE plot, there was a distinct difference between dataset means for all samples before conducting fRMA (Figure @ref(fig:PCA)C). All datasets were rearranged around 0 in the RLE plot after conducting fRMA (Figure @ref(fig:PCA)D). Moreover, there was a clear change in inter-quantile distances, but the values still were over 0.1.

Table 2 Total, up-, and down-regulated DEGs and differentially expressed miRNAs.

	DEGs	up-regulated DEGs	down-regulated DEGs	miRNAs
MI vs. Healthy	860	323	537	hsa-miR-186, miR-21, miR-32
CAD vs. Healthy	670	262	408	hsa-miR-186, miR-21, miR-32
MI vs. CAD	260	144	116	hsa-miR-186

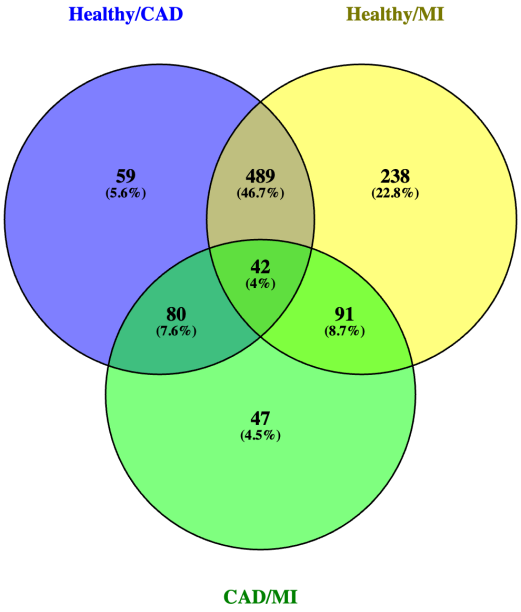

Fig. 2 Venn diagram for DEGs in CAD/Healthy, MI/Healthy, and MI/CAD comparison.

3.2 Differential expression analysis

According to the cutoff criterion of $FDR < 0.05$, there were 860 DEGs between the MI and the healthy samples. Among them, 323 were up-regulated, and 537 were down-regulated in MI compared to the healthy controls. In CAD and healthy groups comparison, we found 670 DEGs, of which 262 and and 408 DEGs were up- and down-regulated, respectively in CAD samples. In the MI and CAD groups, the number of DEGs was 260, and the number of up- and down-regulated genes in MI samples were 144 and 116, respectively in comparison with CAD samples. These data are summarized in Table @ref(tab:DEGstab).

The Venn diagram in Figure @ref(fig:venn) shows that CAD and MI samples share a majority of their DEGs. From 860 DEGs of MI/healthy and 670 DEGs of CAD/healthy, 531 genes were common which is 62% of MI/healthy DEGs and 79% of CAD/healthy DEGs.

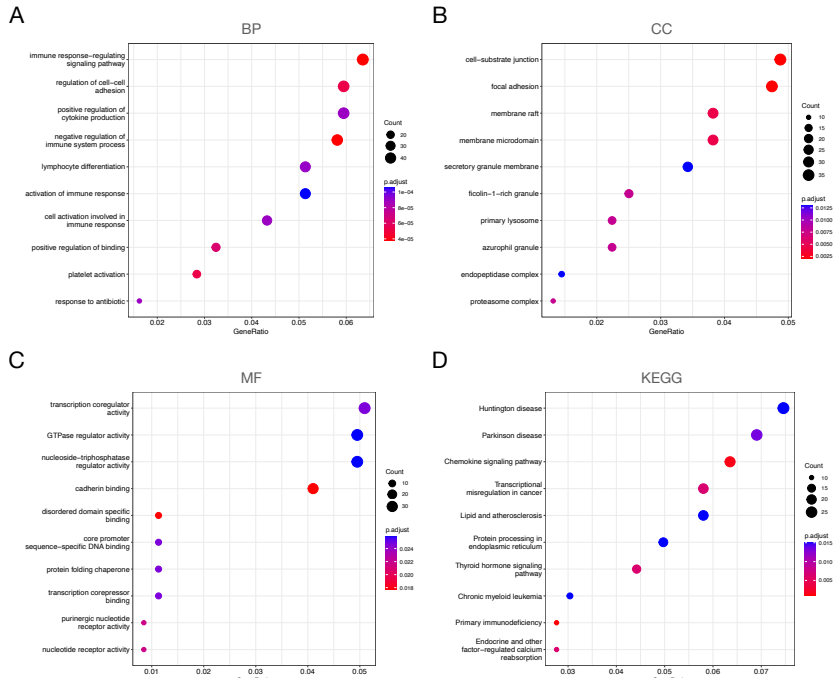

Fig. 3 Gene Ontology (GO) and Kyoto Encyclopedia of Genes and Genomes (KEGG) pathways enriched with the MI and healthy DEGs. (A) Biological process terms. (B) Cellular component terms. (C) Molecular function terms. (D) KEGG analysis.

3.3 Gene ontology (GO) and Kyoto Encyclopedia of Genes and Genomes (KEGG) enrichment analyses of the DEGs.

To explore the biological classification of the DEGs, we performed GO and KEGG pathway enrichment analyses on MI-healthy and CAD-healthy DEGs. In MI versus healthy samples, GO enrichment analysis in the BP category, suggested that the DEGs were enriched in “immune response-regulating signaling pathway”, “lymphocyte differentiation”, “immune response-regulating cell surface receptor signaling pathway”, and “leukocyte activation involved in immune response” (Figure @ref(fig:MIHEnrich)A). In the CC category, the DEGs were enriched in “secretory granule membrane”, “azurophil granule”, “ficolin-1-rich granule”, “tertiary granule”, and “ficolin-1-rich granule membrane” (Figure @ref(fig:MIHEnrich)B). In the MF category, the DEGs were involved in “cadherin binding” and “MHC class I protein binding” (Figure @ref(fig:MIHEnrich)C). KEGG pathway analysis indicated that the DEGs were related to the following pathways: “Chemokine signaling pathway”, “Lipid and atherosclerosis”, and “Hematopoietic cell lineage” (Figure @ref(fig:MIHEnrich)D).

The enrichment results for DEGs of CAD versus healthy samples were as follows. In the BP category, GO enrichment suggested that the DEGs were enriched in “positive regulation of defense response”, “positive regulation of

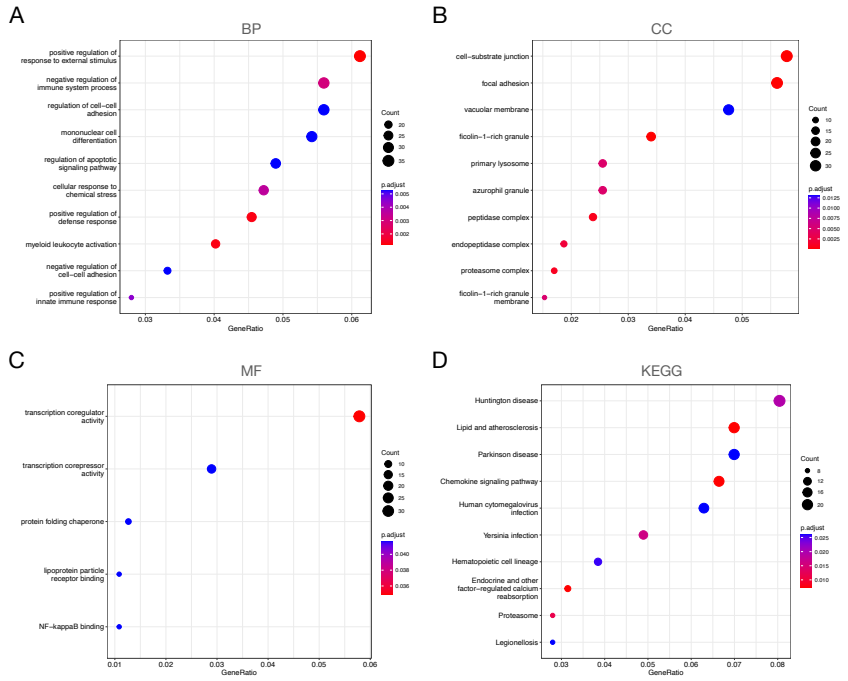

Fig. 4 Gene Ontology (GO) and Kyoto Encyclopedia of Genes and Genomes (KEGG) pathways enriched with the CAD and healthy DEGs. (A) Biological process terms. (B) Cellular component terms. (C) Molecular function terms. (D) KEGG analysis.

innate immune response", "mononuclear cell differentiation", and "positive regulation of response to external stimulus" (Figure @ref(fig:CADHEnrich)A). In the CC category, the DEGs were enriched in "azurophil granule", "ficolin-1-rich granule", and "ficolin-1-rich granule membrane" (Figure @ref(fig:CADHEnrich)B). In the MF category, the DEGs were involved in "lipoprotein particle receptor binding" and "NF-κB binding" (Figure @ref(fig:CADHEnrich)C). KEGG pathway analysis indicated that the DEGs were related to the following pathways: "Chemokine signaling pathway", "Lipid and atherosclerosis", and "Hematopoietic cell lineage" (Figure @ref(fig:CADHEnrich)D).

3.4 Machine Learning

3.4.1 miRNAs in DEGs

Among all DEGs, just miR-186, miR-32, and miR-21 were detected as differentially expressed miRNAs. The expression profile of these three miRNAs is presented in Figure @ref(fig:DEMexp). Additionally, The ROC curves of each miRNA for each layer are presented in Figure @ref(fig:miRROC). Using the logistic regression model the AUC for miR-21, miR-32, and miR-186 was 0.99,

Table 3 Target miRNAs log fold-change and adjusted p-values for CAD samples relative to healthy, MI samples relative to healthy, and MI samples relative to CAD.

	CAD/Healthy		MI/Healthy		MI/CAD	
	logFC	adj. p-value	logFC	adj. p-value	logFC	adj. p-value
miR-186	1.4	3.60e-25	0.9	6.76e-20	-0.5	1.05e-09
miR-21	1.4	1.31e-17	2.3	2.07e-47	0.8	2.96e-11
miR-32	2.5	8.39e-43	2.2	3.10e-59	-0.3	7.60e-04
miR-155	-0.6	2.49e-12	-0.9	7.59e-33	-0.2	2.68e-07
miR-142	0.2	1.90e-01	-0.1	1.70e-01	-0.3	2.90e-04
miR-197	0.5	2.95e-20	0.7	1.59e-47	0.2	8.58e-09
miR-29A	0.7	7.76e-29	0.1	1.70e-01	-0.5	2.14e-10
miR-320C1	0.8	4.72e-22	0.5	1.89e-30	-0.2	1.84e-05

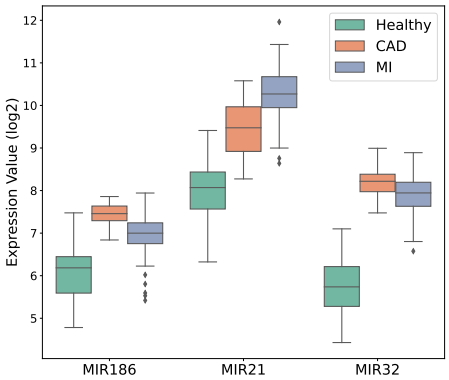

Fig. 5 Expression profile of miR-186, miR-21, and miR32 in Healthy, CAD, and MI samples.

1, and 0.91 respectively (Figure @ref(fig:miRROC)A). Besides, the accuracy of each miRNA for classifying the samples into healthy and not-healthy groups on the test set was 0.92, 0.98, and 0.89 for miR-21, miR-32, and miR-186, respectively. Moreover, the ROC curve of each miRNA for classifying MI and CAD samples was presented in Figure @ref(fig:miRROC)B. For miR-21, miR-32, and miR-186, the AUC and accuracy on the test set were 0.85; 0.7; and 0.82, and 0.78; 0.67; and 0.74, respectively.

First layer for healthy not-healthy isolation: Although single miRNAs had acceptable performance, their predictive value could be improved even further by using them as a set. The ROC curve for the SVM model with an RBF kernel trained with all three miRNAs is presented in Figure @ref(fig:DEMROC)A. The model had a better performance in classification than single miRNAs.The AUC for the model is 1, and its accuracy on the test set was also 1. In Figure @ref(fig:DEMCF)A, the confusion matrix for the model is presented.

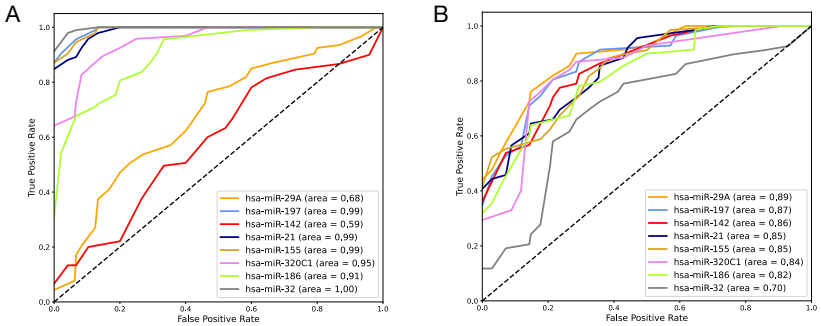

Fig. 6 ROC curve for single miRNAs on test set classification for (A) healthy and not-healthy samples and (B) CAD and MI samples.

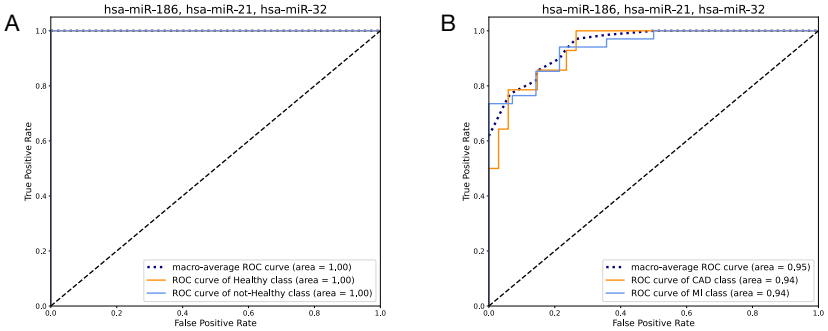

Fig. 7 ROC curve for miRNAs in DEGs on test set classification for (A) healthy and not-healthy samples and (B) CAD and MI samples.

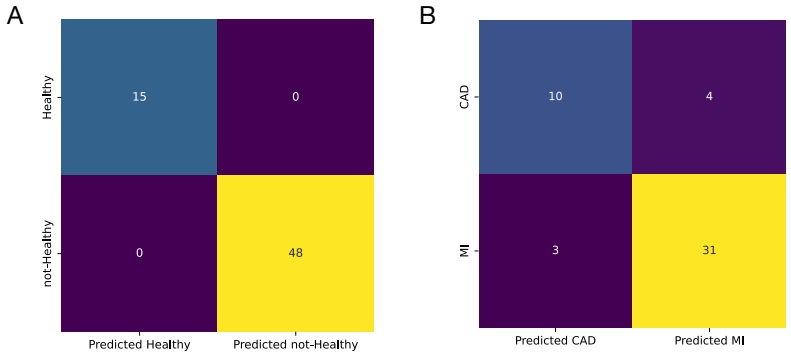

Fig. 8 Confusion matrix on the test set for (A) An SVM model with RBF kernel for healthy and not-healthy and (B) An SVM model with linear kernel for CAD and MI samples classification.

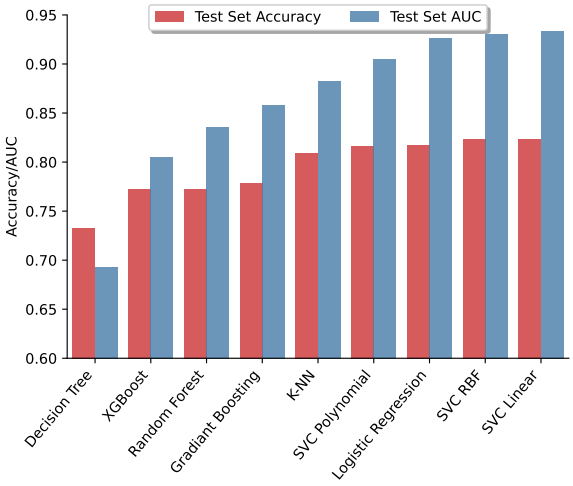

Fig. 9 Area under the curve (AUC) and accuracy of different models trained with three miRNAs in DEGs on the test set.

Table 4 AUC-ROC and accuracy for SVM with the linear kernel as the best model trained with differentially expressed miRNAs on the train and test set before and after hyper-tuning

		Pre-set parameters		Hyper-tuned	
Model	Metrics	train	test	train	test
SVM (Linear Kernel)	AUC-ROC	0.91	0.93	0.92	0.95
	Accuracy	0.83	0.82	0.84	0.85

Second layer for separating MI samples from CAD: Different models were trained using expression values for three differentially miRNAs. The models' 10-fold cross-validated AUC and accuracy on the test set are reported in Figure @ref(fig:DEMmodels). The best model from both AUC and accuracy point-of-view was the SVM model with linear kernel. The AUC and accuracy for this model with its pre-set values were 0.93 and 0.82 respectively. The model was hyper-tuned for C and gamma hyper-parameters, and therefore the model showed better performance. The ROC curve of the hyper-tuned model is presented in Figure @ref(fig:DEMROC)B. For this model the AUC reached 0.95 and the accuracy improved to 0.85 (Table @ref(tab:DEGsML)). Moreover, the sensitivity and specificity for the model on the test set were 0.91 and 0.71 respectively. The confusion matrix for the hyper-tuned model is illustrated in Figure @ref(fig:DEMCF)B.

3.4.2 AUC approach

After calculating the AUC for each miRNA for the classification of MI and CAD samples, miRNAs were sorted, and their performance was investigated

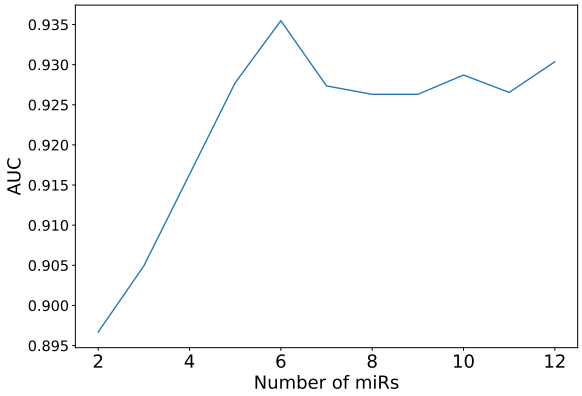

Fig. 10 Area under the curve (AUC) for sets containing an increasing number of miRNAs with the highest individual AUC in MI/CAD separation.

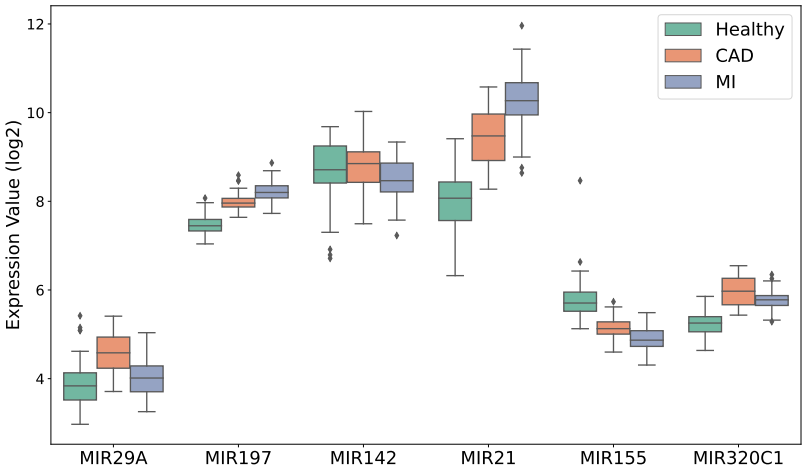

Fig. 11 Expression profile of has-miR-29A, has-miR-197, has-miR-142, has-miR-21, has-miR-155, and has-miR-320C1 in Healthy, CAD, and MI samples.

as a set. The metric of choice for selecting the best set was AUC. As shown in Figure @ref(fig:AUCset), the AUC increased until the number of miRNAs in the set reached six, and after that, it dropped. The AUC for separating MI samples from CAD using these miRNAs was 0.93. The miRNAs in the set were miR-29a, miR-197, miR-142, miR-21, miR-155, and miR-320C1. The expression values of these miRNAs in healthy, CAD, and MI samples are presented in Figure @ref(fig:AUCexp). The ROC curve of the selected miRNAs for MI and CAD sample classification is illustrated in Figure @ref(fig:miRROC)B.

First layer for isolation of healthy and not-healthy samples Using the selected set, an SVM model with an RBF kernel was trained to separate healthy

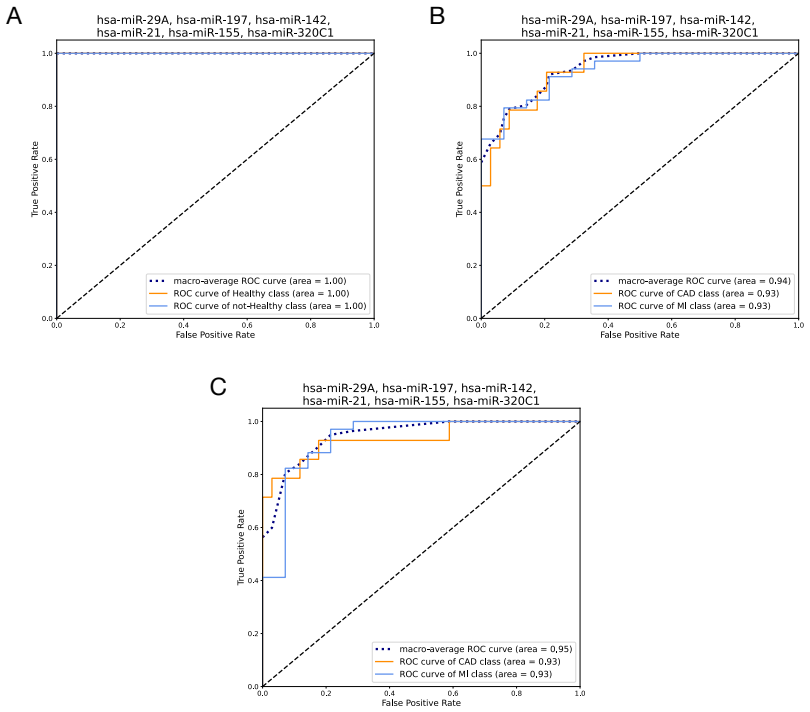

Fig. 12 ROC curve for the set of miRNAs selected by AUC on test set classification. (A) SVM with RBF kernel for healthy and not-healthy samples classification. (B) Logistic regression model for CAD and MI samples classification. (C) SVM with polynomial kernel for CAD and MI samples classification.

from not-healthy samples. The ROC curve for the model is presented in Figure @ref(fig:AUCROC)A and the confusion matrix is illustrated in Figure @ref(fig:AUCCF)A. Both AUC and accuracy for the model on the test set were equal to 1.

Second layer for isolation of MI samples from CAD samples To find the best model for training the best set, different models were trained using their preset values. Their AUC and accuracy results on the test set are presented in Figure @ref(fig:AUCmodels). The best model from the AUC point-of-view was the LR and from the accuracy point-of-view, it was the SVM model with a polynomial kernel. For the LR model the AUC and accuracy were 0.92 and 0.81, respectively; and for the SVM model with a polynomial kernel, the values were 0.91 and 0.84, respectively. Both models were hyper-tuned and the ROC curve for their best performance is presented in Figure @ref(fig:AUCROC)B and C. The AUC and accuracy for the LR model increased to 0.94 and 0.88, respectively. For the SVM model with a polynomial kernel, these values increased to 0.95 and 0.88, respectively (Table @ref(tab:AUCML)). The sensitivity for

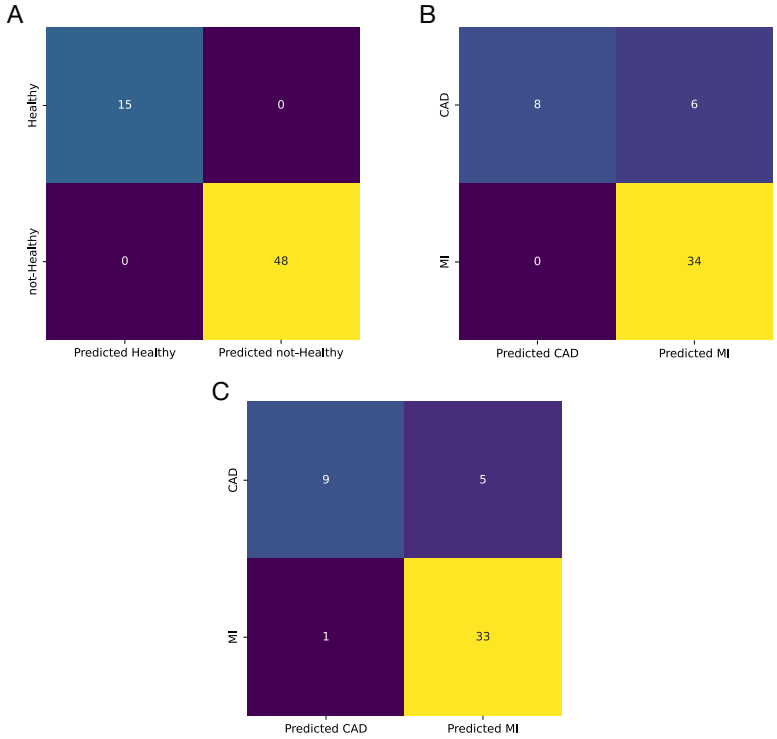

Fig. 13 Confusion matrix on the test set for (A) SVM with RBF kernel for healthy and not-healthy samples classification. (B) Logistic regression model for CAD and MI samples classification. (C) SVM with polynomial kernel for CAD and MI samples classification.

Table 5 AUC-ROC and accuracy for SVM with the linear kernel as the best model trained with miRNAs selected based on their individual AUC-ROC on the train and test set before and after hyper-tuning

		Pre-set parameters		Hyper-tuned	
Model	Metrics	Train	Test	Train	Test
LR	AUC-ROC	0.90	0.92	0.91	0.94
	Accuracy	0.84	0.81	0.84	0.88
SVM (Polynomial Kernel)	AUC-ROC	0.90	0.91	0.91	0.95
	Accuracy	0.86	0.84	0.86	0.88

the LR and SVM models were 1 and 0.97, respectively; and the specificity for them was 0.57 and 0.64, respectively. The confusion matrix for both models is illustrated in Figure @ref(fig:AUCCF)B and C.

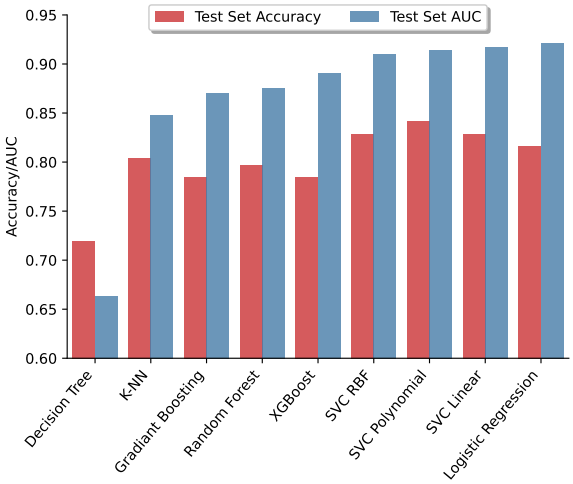

Fig. 14 Area under the curve (AUC) and accuracy of different models trained with three miRNAs in DEGs on the test set.

4 Discussion

The prevalence of acute MI (AMI) can lead to high-rate mortality in the clinical setting. However, early diagnosis and application of suitable treatment protocols can reduce mortality and improve AMI prognosis ("Cardiovascular Diseases (CVDs)" n.d.; Thygesen et al. 2018; Tsao et al. 2022). Studies have suggested that changes in miRNA expression may play a significant role in the progression of MI and the subsequent remodeling (Laggerbauer and Engelhardt 2022). It is believed that the expression of miRNAs is altered during the various biological processes correlated with MI within the myocardium or other related tissues (Khan, Gupta, and Mahapatra 2022). Although several research has been concentrated on examining free circulating miRNAs in the serum samples for the detection of cardiac tissue injuries (Kaur et al. 2020), more information is needed to fully comprehend the miRNAs found in different blood sub-components like plasma, platelets, and PBMCs. Based on previous data, PBMCs are critically involved in plaque destabilization and rupture as well as early inflammatory responses during MI (Mosallaei et al. 2022; Hapke et al. 2022). Moreover, PBMCs have specific miRNA profile that is altered under certain pathological conditions which are great candidates as disease biomarkers (Mosallaei et al. 2022).

PBMCs can respond to several insulting conditions such as MI in the least possible time with prominent changes in their miRNA profile (Mosallaei et al. 2022). Considering the regulatory roles, subtle changes in the transcription of miRNAs can be monitored even before alteration in the levels of mRNAs and proteins (Schulte et al. 2020). These features make the miRNAs an early-stage valid diagnostic tool for the detection of minor and major cell injuries. To date,

few studies have been performed to compare the miRNA profiles in PBMCs belonging to acute MI patients and other CADs and healthy samples to find a robust set of identical miRNAs to differentiate these pathological conditions.

In this study, we combined three GEO datasets of healthy, CAD, and MI samples. Having these samples set alongside bioinformatics analysis and ML means, it is possible to identify potential biomarker sets and also effective therapeutic targets. The results of the DEG analysis (Table @ref(tab:DEGstab) and Figure @ref(fig:venn)) are proof of the close relationship between the MI and CAD samples. Interestingly, functional enrichment analysis demonstrated that DEGs in both healthy/CAD and healthy/MI were strongly correlated to immune cell response which is a major cellular part of PBMCs. Here, two different sets of miRNAs were used as biomarker sets for sample classification. miR-21; miR-32; and miR-186 were selected as differentially expressed miRNAs, and miR-21; miR-29a; miR-142; miR155; miR-197; and miR-320c1 were selected according to their AUC values. As shown in Figure @ref(fig:miRROC), all other miRNAs selected with both approaches had AUC-ROC over 0.9 for the isolation of healthy and not-healthy samples except for miR-142 and miR-29a. Data confirmed that the real challenge is to classify CAD and MI samples because of close overlap. Of 8 miRNAs under investigation in both approaches except for miR-32, all miRNAs had an AUC-ROC over 0.8 for the discrimination of CAD and MI samples. Besides, the high AUC-ROC values of miRNAs confirms their high potential as biomarkers.

ML models when trained with miRNA sets selected by both DEG and AUC approaches showed better performance in the classification than each miRNA. To avoid unwanted complexity and poor predictive values, a two-layer architecture was also designed. The first layer was for for the discrimination of healthy from not-healthy samples, and the second layer separated the CAD from MI candidates. As expected in both approaches, a hyper-tuned SVM model could flawlessly separates healthy from not-healthy samples using distinct miRNAs sets. The ML models were also capable of effectively separating CAD from MI patients. Although both miRNA sets had nearly the same AUC-ROC with their best model, the accuracy, sensitivity, and specificity were different. The model trained with DEGs had better specificity, but the one trained with AUC-selected miRNAs had slightly better accuracy and higher sensitivity. This difference comes from the different strategies the selection of biomarkers sets.

Numerous studies have reported different biological processes can affect the expression of miRNAs in PBMCs. However, there are still controversies regarding the exact role of miRNAs in the function of immune cells and the correlation of specific pathological conditions with miRNA profiles. Several studies have proved the activation of specific miRNA types in PBMCs under cardiovascular events (S. Li et al. 2015; Yao et al. 2016; Liu et al. 2017; Horita, Farquharson, and Stephen 2021; Cai et al. 2020; Zhao et al. 2018; Bhansali et al. 2022). For instance, there is evidence that the elevation of miR-186 suppresses the expression of Cystathionine-γ-lyase, leading to the subsequent secretion of pro-inflammatory cytokines and cellular lipid accumulation. Be-

sides, macrophage-derived miR-186 may promote atherosclerotic plaques (Yao et al. 2016). In line with this claim, we found that miR-186 is up-regulated in both CAD and MI candidates related to control counterparts. Surprisingly, the obtained data indicated that the expression of miR-186 is higher in CAD patients in comparison to MI (Figure @ref(fig:DEMexp)), To be specific, miR-186 is the only differentially expressed miRNA between CAD and MI, indicating its main role in the promotion of atherosclerosis.

As mentioned before, miR-21 was also up-regulated in both MI and CAD patients in comparison to healthy controls. Moreover, the expression value of miR-21 was significantly higher in MI than that of the CAD group (Table @ref(tab:mirExptable)). It is thought that the up-regulation of miRNA-21 in PBMCs is a compensatory reaction to reduce T_{reg} lymphocyte number in response to the reduction of TGFβ1 secretion into the plasma through a TGFβ1/smad-independent pathway. In line with previous and present data, miR-21 can modulate the activity of PBMCs following the occurrence of cardiovascular diseases (S. Li et al. 2015).

Recent data have supported the elevation of miR-32 in CAD patients with the calcification of coronary artery. Of note, miR-32 stimulates the calcification of mouse vascular smooth muscle through the regulation of bone morphogenetic protein-1, runt-related transcription factor-2 (RUNX2), osteopontin, and bone-specific phosphoprotein matrix GLA protein (Liu et al. 2017). Likewise, there are some reports associated with the activity of PBMC miR-32 under several pathologies (Zeng et al. 2021; Wang et al. 2020). The exact role of PBMC miR-32 after cardiovascular events remained to be elucidated.

Molecular analyses have indicated the regulatory role of miRNAs selected by the AUC approach in PBMCs after a cardiovascular event. As the only common miRNA of the two sets, molecular function of miR-21 in CVDs was covered in DEGs miRNA set. Based on numerous reports mir-29a can be activated in different diseases (Horita, Farquharson, and Stephen 2021).Data analysis indicated that miR-29a is significantly up-regulated in CAD patients in comparison to healthy and MI groups (Table @ref(tab:mirExptable)). Increased miR-29a is associated with the progression of atherosclerosis, and the combination of miR-29a and ox-LDL was offered as a valid biomarker set for paraclinical classification (Huang et al. 2016). However, the role of miR-29a in the function of PBMCs in CAD patients has not been completely examined.

According to the present data (Table @ref(tab:mirExptable)), the difference in miR-142 expression between MI/Healthy and CAD/Healthy was not significant, but these values reached statistically significant in MI as compared to CAD. Based on different reports, miR-142 is commonly active in PBMCs. This miRNA directly targets and inhibits the expression of Adenomatous Polyposis Coli, a negative WNT signaling pathway regulator, contributing to the activation of the WNT signaling pathway and cardiac fibroblast activation after myocardial ischemia (Cai et al. 2020).

We also noted that miR-155 is the only down-regulated miRNA among all miRNAs in both CAD/healthy and MI/Healthy comparisons (Table @ref(tab:mirExptable)). There are numerous reports on the down-regulation of miR-155 in PBMCs af-

ter MI or in CAD patients. Previous data suggested an inverse relationship between miR-155 levels and the severity of the coronary artery condition (Zhang et al. 2015; Zhao et al. 2018). Along with current data and previous findings, it is postulated that miR-155 has a protective effect under pathological conditions. This genetic element can control inflammation and thus reduce tissue damage through its negative feedback effects on inflammatory factors. These features coincide with the reduction of atherosclerosis (Zhang et al. 2015).

Data indicated that miR-197 is also significantly up-regulated in both CAD/healthy and MI/healthy groups. In previous studies, it has been shown that miRNA-197 may play a critical role in regulating the anti-inflammatory response of IL-35 by affecting pro/ anti-inflammatory cytokine secretion, M1/M2 macrophage ratio, T_{reg} lymphocyte proliferation, and T cell suppression suggesting the potential diagnostic role of miR-197 in adverse cardiovascular events (Bhansali et al. 2022). There are some reports about miR-320 role in the physiopathology of cardiac fibrosis. Mechanistically, Molecular analyses revealed that miR-320 might induce various effects by targeting PLEKHM3 and IFITM1 in cardiomyocytes and cardiac fibroblasts, respectively (F. Li et al. 2021). However, there are no reports on miR-320c1 activity in the cardiovascular system or PBMCs.

5 Conclusion

In summary, we derived a set of miRNA biomarkers by comparing MI samples to both healthy and CAD samples. We found that the SVM model performed best in both the first layer, which separated healthy and not-healthy samples, and the second layer, which classified MI/CAD samples. The set of miRNAs selected based on their AUC values had slightly better performance in the second layer. Overall, our two-layer structure achieved a weighted accuracy of 0.91. This demonstrates the potential for combining bioinformatics and machine learning techniques to identify novel biomarkers and gain a deeper understanding of myocardial infarction.

6 References

$$a^2 + b^2 = c^2 \tag{1}$$

Bhansali, Shipra, Amit Kumar Yadav, Chetan Bakshi, and Veena Dhawan. 2022. “Interleukin-35 Mitigates Ox-LDL-Induced Proatherogenic Effects via Modulating miRNAs Associated with Coronary Artery Disease (CAD).” *Cardiovascular Drugs and Therapy*, April. https://doi.org/10.1007/s10557-022-07335-x.

Cai, Lidong, Gong Chao, Weifeng Li, Jumo Zhu, Fangfang Li, Baozhen Qi, Yong Wei, et al. 2020. “Activated Cd4+ T Cells-Derived Exosomal miR-142-3p Boosts Post-Ischemic Ventricular Remodeling by Activating My-

ofibroblast." *Aging* 12 (8): 7380–96. https://doi.org/10.18632/aging.103084.

Canali, Raffaella, Lucia Natarelli, Guido Leoni, Elena Azzini, Raffaella Comitato, Oezgur Sancak, Luca Barella, and Fabio Virgili. 2014. "Vitamin C Supplementation Modulates Gene Expression in Peripheral Blood Mononuclear Cells Specifically Upon an Inflammatory Stimulus: A Pilot Study in Healthy Subjects." *Genes & Nutrition* 9 (3): 390. https://doi.org/10.1007/s12263-014-0390-x.

"Cardiovascular Diseases (CVDs)." n.d. Accessed March 12, 2023. https://www.who.int/news-room/fact-sheets/detail/cardiovascular-diseases-(cvds).

Gao, Jie, Jia Liu, Ying Zhang, BaoYi Guan, Hua Qu, Hua Chai, WenTing Wang, XiaoJuan Ma, and DaZhuo Shi. 2020. "PBMCs-Derived microRNA Signature as a Prethrombotic Status Discriminator in Stable Coronary Artery Disease." *Thrombosis and Haemostasis* 120 (01): 121–31. https://doi.org/10.1055/s-0039-1700518.

Hapke, Nils, Margarete Heinrichs, DiyaaElDin Ashour, Elena Vogel, Ulrich Hofmann, Stefan Frantz, and Gustavo Campos Ramos. 2022. "Identification of a Novel Cardiac Epitope Triggering T-Cell Responses in Patients with Myocardial Infarction." *Journal of Molecular and Cellular Cardiology* 173 (December): 25–29. https://doi.org/10.1016/j.yjmcc.2022.09.001.

Harris, Charles R., K. Jarrod Millman, Stéfan J. van der Walt, Ralf Gommers, Pauli Virtanen, David Cournapeau, Eric Wieser, et al. 2020. "Array Programming with NumPy." *Nature* 585 (7825): 357–62. https://doi.org/10.1038/s41586-020-2649-2.

Head, Tim, Manoj Kumar, Holger Nahrstaedt, Gilles Louppe, and Iaroslav Shcherbatyi. 2021. *Scikit-Optimize/Scikit-Optimize* (version v0.9.0). Zenodo. https://doi.org/10.5281/zenodo.5565057.

Horita, Masahiro, Colin Farquharson, and Louise A Stephen. 2021. "The Role of miR-29 Family in Disease." *Journal of Cellular Biochemistry* 122 (7): 696–715. https://doi.org/10.1002/jcb.29896.

Huang, Yu-Qing, An-Ping Cai, Ji-Yan Chen, Cheng Huang, Jie Li, and Ying-Qing Feng. 2016. "The Relationship of Plasma miR-29a and Oxidized Low Density Lipoprotein with Atherosclerosis." *Cellular Physiology and Biochemistry* 40 (6): 1521–28. https://doi.org/10.1159/000453202.

Kalayinia, Samira, Fateme Arjmand, Majid Maleki, Mahshid Malakootian, and Chandra Pal Singh. 2021. "MicroRNAs: Roles in Cardiovascular Development and Disease." *Cardiovascular Pathology* 50 (January): 107296. https://doi.org/10.1016/j.carpath.2020.107296.

Kaur, Amanpreet, Sharon T Mackin, Kenny Schlosser, Fui Lin Wong, Malik Elharram, Christian Delles, Duncan J Stewart, Natalie Dayan, Tara Landry, and Louise Pilote. 2020. "Systematic Review of microRNA Biomarkers in Acute Coronary Syndrome and Stable Coronary Artery Disease." *Cardiovascular Research* 116 (6): 1113–24. https://doi.org/10.1093/cvr/cvz302.

Khan, Abrar A., Vinayak Gupta, and Nitish R. Mahapatra. 2022. "Key Regulatory miRNAs in Lipid Homeostasis: Implications for Cardiometabolic Diseases and Development of Novel Therapeutics." *Drug Discovery Today* 27 (8): 2170–80. https://doi.org/10.1016/j.drudis.2022.05.003.

Laggerbauer, Bernhard, and Stefan Engelhardt. 2022. "MicroRNAs as Therapeutic Targets in Cardiovascular Disease." *Journal of Clinical Investigation* 132 (11): e159179. https://doi.org/10.1172/JCI159179.

Lazar, C., S. Meganck, J. Taminau, D. Steenhoff, A. Coletta, C. Molter, D. Y. Weiss-Solis, R. Duque, H. Bersini, and A. Nowe. 2013. "Batch Effect Removal Methods for Microarray Gene Expression Data Integration: A Survey." *Briefings in Bioinformatics* 14 (4): 469–90. https://doi.org/10.1093/bib/bbs037.

Li, Fang, Shan-Shan Li, Hui Chen, Jian-Zhi Zhao, Jie Hao, Jin-Ming Liu, Xiu-Guang Zu, and Wei Cui. 2021. "miR-320 Accelerates Chronic Heart Failure with Cardiac Fibrosis Through Activation of the Il6/Stat3 Axis." *Aging* 13 (18): 22516–27. https://doi.org/10.18632/aging.203562.

Li, Sihui, Qian Fan, Shaolin He, Tingting Tang, Yuhua Liao, and Jiangjiao Xie. 2015. "MicroRNA-21 Negatively Regulates Treg Cells Through a TGF-β1/Smad-Independent Pathway in Patients with Coronary Heart Disease." *Cellular Physiology and Biochemistry* 37 (3): 866–78. https://doi.org/10.1159/000430214.

Liu, Jianghua, Xinhua Xiao, Yingying Shen, Ling Chen, Canxin Xu, Heng Zhao, Ying Wu, et al. 2017. "MicroRNA-32 Promotes Calcification in Vascular Smooth Muscle Cells: Implications as a Novel Marker for Coronary Artery Calcification." Edited by Yin Tintut. *PLOS ONE* 12 (3): e0174138. https://doi.org/10.1371/journal.pone.0174138.

Maciejak, Agata, Marek Kiliszek, Marcin Michalak, Dorota Tulacz, Grzegorz Opolski, Krzysztof Matlak, Slawomir Dobrzycki, Agnieszka Segiet, Monika Gora, and Beata Burzynska. 2015. "Gene Expression Profiling Reveals Potential Prognostic Biomarkers Associated with the Progression of Heart Failure." *Genome Medicine* 7 (1): 26. https://doi.org/10.1186/s13073-015-0149-z.

Matone, Alice, Colm M. O'Grada, Eugene T. Dillon, Ciara Morris, Miriam F. Ryan, Marianne Walsh, Eileen R. Gibney, et al. 2015. "Body Mass Index Mediates Inflammatory Response to Acute Dietary Challenges." *Molecular Nutrition & Food Research* 59 (11): 2279–92. https://doi.org/10.1002/mnfr.201500184.

McCall, M. N., B. M. Bolstad, and R. A. Irizarry. 2010. "Frozen Robust Multiarray Analysis (fRMA)." *Biostatistics* 11 (2): 242–53. https://doi.org/10.1093/biostatistics/kxp059.

McCall, Matthew N., Karan Uppal, Harris A. Jaffee, Michael J. Zilliox, and Rafael A. Irizarry. 2011. "The Gene Expression Barcode: Leveraging Public Data Repositories to Begin Cataloging the Human and Murine Transcriptomes." *Nucleic Acids Research* 39 (suppl_1): D1011–15. https://doi.org/10.1093/nar/gkq1259.

McKinney, Wes. 2010. "Data Structures for Statistical Computing in Python." In *Proceedings of the 9th Python in Science Conference*, edited by Stéfan van der Walt and Jarrod Millman, 56–61. https://doi.org/ 10.25080/Majora-92bf1922-00a .

Mosallaei, Meysam, Naeim Ehtesham, Shima Rahimirad, Mostafa Saghi, Nasim Vatandoost, and Sharifeh Khosravi. 2022. "PBMCs: A New Source of Diagnostic and Prognostic Biomarkers." *Archives of Physiology and Biochemistry* 128 (4): 1081–87. https://doi.org/10.1080/13813455.2020.1752257.

Pedregosa, F., G. Varoquaux, A. Gramfort, V. Michel, B. Thirion, O. Grisel, M. Blondel, et al. 2011. "Scikit-Learn: Machine Learning in Python." *Journal of Machine Learning Research* 12: 2825–30.

Reel, Parminder S., Smarti Reel, Ewan Pearson, Emanuele Trucco, and Emily Jefferson. 2021. "Using Machine Learning Approaches for Multi-Omics Data Analysis: A Review." *Biotechnology Advances* 49 (July): 107739. https://doi.org/10.1016/j.biotechadv.2021.107739.

Schulte, Christian, Temo Barwari, Abhishek Joshi, Tanja Zeller, and Manuel Mayr. 2020. "Noncoding RNAs Versus Protein Biomarkers in Cardiovascular Disease." *Trends in Molecular Medicine* 26 (6): 583–96. https://doi.org/10.1016/j.molmed.2020.02.001.

Schulte, Christian, Mahir Karakas, and Tanja Zeller. 2017. "microRNAs in Cardiovascular Disease – Clinical Application." *Clinical Chemistry and Laboratory Medicine (CCLM)* 55 (5). https://doi.org/10.1515/cclm-2016-0576.

Soler-Botija, Carolina, Carolina Gálvez-Montón, and Antoni Bayés-Genís. 2019. "Epigenetic Biomarkers in Cardiovascular Diseases." *Frontiers in Genetics* 10 (October): 950. https://doi.org/10.3389/fgene.2019.00950.

Thygesen, Kristian, Joseph S. Alpert, Allan S. Jaffe, Bernard R. Chaitman, Jeroen J. Bax, David A. Morrow, Harvey D. White, and The Executive Group on behalf of the Joint European Society of Cardiology (ESC)/American College of Cardiology (ACC)/American Heart Association (AHA)/World Heart Federation (WHF) Task Force for the Universal Definition of Myocardial Infarction. 2018. "Fourth Universal Definition of Myocardial Infarction (2018)." *Circulation* 138 (20). https://doi.org/10.1161/CIR.0000000000000617.

Torun, Furkan M., Sebastian Virreira Winter, Sophia Doll, Felix M. Riese, Artem Vorobyev, Johannes B. Mueller-Reif, Philipp E. Geyer, and Maximilian T. Strauss. 2023. "Transparent Exploration of Machine Learning for Biomarker Discovery from Proteomics and Omics Data." *Journal of Proteome Research* 22 (2): 359–67. https://doi.org/10.1021/acs.jproteome.2c00473.

Tsao, Connie W., Aaron W. Aday, Zaid I. Almarzooq, Alvaro Alonso, Andrea Z. Beaton, Marcio S. Bittencourt, Amelia K. Boehme, et al. 2022. "Heart Disease and Stroke Statistics—2022 Update: A Report From the American Heart Association." *Circulation* 145 (8). https://doi.org/10.1161/CIR.0000000000001052.

Wang, Dan, Ting Zeng, Zhi Lin, Lu Yan, Fenglin Wang, Lanlan Tang, Leyuan Wang, Daolin Tang, Pan Chen, and Minghua Yang. 2020. "Long Non-Coding RNA Snhg5 Regulates Chemotherapy Resistance Through the miR-32/Dnajb9 Axis in Acute Myeloid Leukemia." *Biomedicine & Pharmacotherapy* 123 (March): 109802. https://doi.org/10.1016/j.biopha.2019.109802.

Yao, Yan, Xin Zhang, Hai-peng Chen, Liang Li, Wei Xie, Gang Lan, Zhenwang Zhao, Xi-Long Zheng, Zong-bao Wang, and Chao-ke Tang. 2016. "MicroRNA-186 Promotes Macrophage Lipid Accumulation and Secretion of Pro-Inflammatory Cytokines by Targeting Cystathionine γ-Lyase in THP-1 Macrophages." *Atherosclerosis* 250 (July): 122–32. https://doi.org/10.1016/j.atherosclerosis.2016.04.030.

Yap, Jonathan, Jason Irei, Javier Lozano-Gerona, Selena Vanapruks, Tianmai Bishop, and William A. Boisvert. 2023. "Macrophages in Cardiac Remodelling After Myocardial Infarction." *Nature Reviews Cardiology*, January. https://doi.org/10.1038/s41569-022-00823-5.

Zeng, Zl, Qingyun Zhu, Zhibo Zhao, Xuyu Zu, and Jianghua Liu. 2021. "Magic and Mystery of microRNA-32." *Journal of Cellular and Molecular Medicine* 25 (18): 8588–8601. https://doi.org/10.1111/jcmm.16861.

Zhang, Yu-Hui, Liang-Hua Xia, Jia-Mei Jin, Ming Zong, Ming Chen, and Bo Zhang. 2015. "Expression Level of miR–155 in Peripheral Blood." *Asian Pacific Journal of Tropical Medicine* 8 (3): 214–19. https://doi.org/10.1016/S1995-7645(14)60318-7.

Zhao, Duo, Jing Zhao, Jiangbin Sun, Yanling Su, Jinfeng Jian, Huaan Ye, Jiawang Lin, Zongda Yang, Jiatao Feng, and Zhiping Wang. 2018. "The Expression Level of miR-155 in Plasma and Peripheral Blood Mononuclear Cells in Coronary Artery Disease Patients and the Associations of These Levels with the Apoptosis Rate of Peripheral Blood Mononuclear Cells." *Experimental and Therapeutic Medicine*, September. https://doi.org/10.3892/etm.2018.6797.